Toxicology Research

Accepted Manuscript

ROYAL SOCIETY OF CHEMISTRY

www.rsc.org/toxicology

Health hazard of the Methylammonium Lead Iodide Based Perovskites: cytotoxicity studies

Iness R. Benmessaoud[1], Anne-Laure Mahul-Mellier[2], Endre Horvath[1], Bohumil Maco[2], Massimo Spina[1], Hilal A. Lashuel[2*], Làszló Forró[1*]

[1]Laboratory of Physics of Complex Matter, Ecole Polytechnique Fédérale de Lausanne (EPFL), 1015 Lausanne, Switzerland.

[2] Laboratory of Molecular and Chemical Biology of Neurodegeneration, EPFL, 1015 Lausanne, Switzerland.

* Corresponding authors:

Email: laszlo.forro@epfl.ch, Tel: +41216934306

Email: hilal.lashuel@epfl.ch, Tel:+41 21 69 39691

Keywords: hybrid halide photovoltaic perovskite, toxicity, apoptois, mitochondrial activity

Abstract

New technologies launch novel materials; beside their performances in products, their health hazard must be tested. This applies to the lead halide perovskite $CH_3NH_3PbI_3$ as well, which offers fulgurate applications in photovoltaic devices. We report the effects of $CH_3NH_3PbI_3$ photovoltaic perovskite in human lung adenocarcinoma epithelial cells (A549) human dopaminergic neuroblastoma cells (SH-SY5Y) and murine primary hippocampal neurons by using multiple assays and electron microscopy studies. In cell culture media the major part of the dissolved $CH_3NH_3PbI_3$ and has a strong cell-type dependent effect. Hippocampal primary neurons and neuroblastoma cells suffer a massive apoptotic cell death, whereas exposure to lung epithelial cells dramatically alters kinetics of proliferation, metabolic activity and cellular morphology without inducing noticeable cell death. Our findings underscore the critical importance of conducting further studies to investigate the effect of short and long-term exposure to $CH_3NH_3PbI_3$ on health and environment.

1. Introduction

Solar energy remains one of the most promising alternative sources to supply electricity. However, after decades of research and three generations of solar cell devices, solar power still represents less than 1% in the global energy chart. Nevertheless, the International Energy Agency (IEA) predicts a spectacular increase in the worldwide photovoltaic energy production by mid-century. Therefore, intensive research and investments have been made to develop novel materials that are used in the production of the next generation of photovoltaic cells offering more efficient and cost effective materials with enhanced performance and improved architecture.

The latest breakthrough is due to the organometallic halide perovskite $CH_3NH_3PbI_3$ (hereafter $MAPbI_3$ for methylammonium lead iodide)[1–4]. $MAPbI_3$ represents such novel materials and offers several advantages that have led to their wide-spread use and application in photovoltaic cells: it is 1) made of inexpensive components; 2) very robust and flexible; 3) easy to manufacture a photovoltaic cell, and 4) extremely efficient in converting sunlight to electricity. Aside from its remarkable performance in photovoltaic cells[5–7], this material seems to be very promising in solar water splitting[8] and optoelectronic devices like LEDs[9], lasers[10] and photodetectors[11]. It has been estimated that mass manufacturing of this material in industrial facilities could begin as soon as 2018.

The high toxicity of lead[12–15] combined with the expected extensive use of organometallic halide perovskite $CH_3NH_3PbI_3$ raises major concerns about the potential health hazards and consequences of short, medium and long-term exposure to this material. Studies on acute and chronic lead exposure of humans[13,16], laboratory animals[17,18] and plants[19] showed that the lowest exposure level resulted in detectable effects, bioaccumulation and poisoning. In the case of $MAPbI_3$, not only human exposure during device production and handling is a concern, but its release into the environment, soil and waterways, after failure of large area solar cells (due to a potential thermal shock or damaged encapsulation)[20] also represents major health and environmental risks. In addition to lead toxicity, iodine[21,22] and methylamine[23–25] might cause a

health hazard, as well. Taken together, these observations emphasize the critical importance of investigating the effect of $MAPbI_3$ exposure at the cellular and organism levels before its large-scale exploitation.

One of the main access routes of $MAPbI_3$ to the human body is by inhalation[26] of its volatile nanoparticles. The airborne material can be deposited in the respiratory path, nose, bronchi, and lung getting into contact with epithelial cells. The material can be dissolved in body fluids and through the blood stream or olfactory nerves, can then reach the brain[12,13,27,28]. Thus we were particularly interested in evaluating the effects of $MAPbI_3$ in various cellular models including human lung adenocarcinoma epithelial cells (A549), human dopaminergic neuroblastoma cells (SH-SY5Y) and murine primary hippocampal neurons.

Remarkably, the effect of $MAPbI_3$ appeared to be cell-type dependent. Primary neurons and neuroblastoma cells' exposure to $MAPbI_3$ induced massive apoptotic cell death, whereas exposure of the A549 epithelial cells dramatically affected their kinetics of proliferation, their metabolic activity and cellular morphology without inducing noticeable cell death.

Altogether, our findings provide novel insights into the cellular mechanisms by which the potential bioaccumulation of $MAPbI_3$ could induce health hazards on the long term. Our data emphasize the critical importance of performing further studies (e.g. in living organisms, to apply additional experimental models) and also point-out the need to improve the device architecture by robust confinement of the material.

2. Experimental Results

2.1 Preparation and characterization of $MAPbI_3$ and its solution

$MAPbI_3$ can be synthesized in various forms: big crystals, nano-crystals in thin films, nanowires, or quantum dots depending on the purpose of their use (Fig. 1a, lower part). All these forms stem from a solution-based process described by Poglitch and Weber[29]. A macroscopic amount that was prepared for this study is shown in the upper part of Fig. 1a.

As a first step towards assessing the potential toxicity of $MAPbI_3$, it is important to conduct quantitative assessment of their volatility and stability to chemical and microbial degradation. It is well known that $MAPbI_3$ has a hygroscopic character i.e. is sensitive to moisture and decomposes into its water-soluble constituents. Therefore, the solubility of $MAPbI_3$ polycrystalline powder was determined in deionized water (close to outdoor environmental conditions) as well as in two types

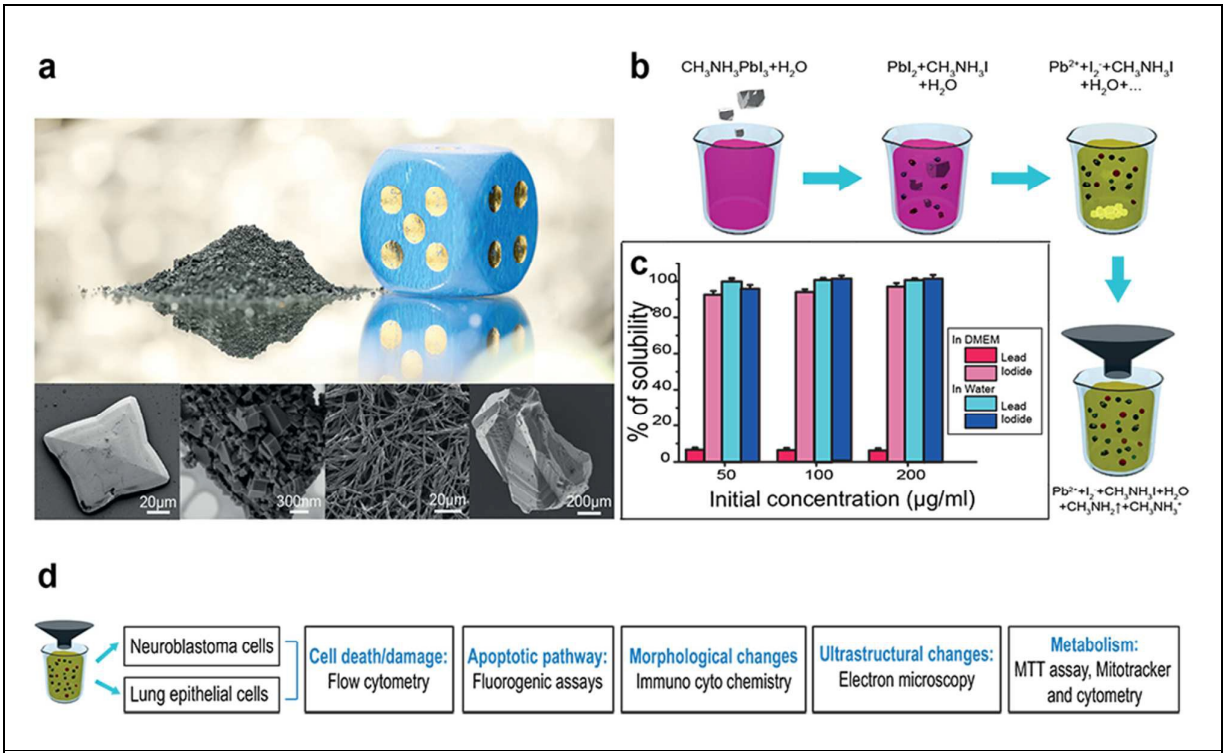

Fig 1. The $MAPbI_3$ perovskite and its preparation for the toxicity tests.
(a) The different morphological appearances of the material (lower panel) and the typical quantity of microcrystals used for the present study (upper panel; the dice in the background sets the scale); **(b)** The different steps of the solution preparation in water or in cell culture medium (DMEM). Note that in the last one, the majority of the Pb^{2+} ions precipitates in a yellow/white deposit consisting of lead-phosphate and lead carbonate (see Supplementary Fig. S2); **(c)** Concentration levels of lead and iodine in water and in cell culture medium after filtration; **(d)** Chart of the toxicity study of $MAPbI_3$ on neuronal and epithelial cells with the major techniques and the expected information obtained.

of cell culture medium (DMEM and DMEM:F12, mimicking the human body fluid conditions). The perovskite powder was dispersed in these liquids at different concentrations (from 50 to 3000 µg/ml). These solutions were then filtered and analyzed by inductively coupled plasma atomic

emission spectroscopy (ICP-AES) at various time points (1-30 days). The initial step of the perovskite dissolution was identical in deionized water and in cell culture media. In contact with the liquids, the initially silver-grey colored $MAPbI_3$ was decomposed into solid, yellow PbI_2 and water-soluble methyl ammonium iodide derivatives within few seconds. Importantly, altered dissolution mechanisms were observed on longer soaking times. At the highest dose, clear and transparent liquid was obtained in deionized water after 4 days, indicating that the PbI_2 was completely dissolved. In contrast, in cell culture media, white precipitate and a reduced amount of water-soluble Pb^{2+} (6%) was observed, even 30 days post-preparation (Fig. 1 b-c and Supplementary Fig. S1). Elemental analysis confirmed that the white, solid precipitate is composed of a mixture of lead (II) hydroxide, lead (II) carbonate, and lead (II) phosphate compounds (Supplementary Fig. S2), which were formed by the reaction of Pb^{2+} with the carbonate, phosphate and hydroxide anions of the cell culture media. These marked differences in the dissolution of $MAPbI_3$ in water and cell culture media clearly demonstrate that its potential environmental impact can be modulated by different parameters (temperature, pH and chemical environment dependent equilibrium of soluble and solid forms). We targeted concentrations of 50, 100 and 200 μg/ml of $MAPbI_3$, which were administrated to cell cultures on time scales extended to few days. A solution of $MAPbI_3$ at 100 μg/ml has a molecular weight percent of lead, iodine and methylamine of respectively 33.42, 61.41 and 5.17%. As seen in Fig. 1c, the culture media, where $MAPbI_3$ was added then filtered, contain more than 90% of the initial iodine and 6% of the initial lead. Methylamine is known to be soluble[30] in a water-rich environment and cannot be quantified using elemental analysis due to the presence of carbon, hydrogen and nitrogen. For simplicity, the nominal $MAPbI_3$ concentration is used on the histograms and figures.

Figure 1d provides an overview of our experimental design and methods used to assess $MAPbI_3$ toxicity. Only the filtered, cell culture medium soluble part of $MAPbI_3$ was administrated to the cell lines A549, SH-SY5Y and the murine primary hippocampal neurons. The effects of $MAPbI_3$ exposure were measured by flow cytometry, fluorogenic and colorimetric assays, immunocytochemistry (ICC) and transmission electron microscopy (TEM). The combination and complementarity of these assays allowed for assessing the effect of $MAPbI_3$ on cellular

properties, metabolic activity, morphology and viability. Interestingly, the two cell types have radically a different response to $MAPbI_3$ exposure. The details of these observations are given below.

2.2 $MAPbI_3$ induces apoptotic cell death in SH-SY5Y cell line and mice hippocampal primary neurons

We first evaluated the time and concentration dependent effects of $MAPbI_3$ in neuroblastoma SH-SY5Y cells. $MAPbI_3$ was administered to cells at concentrations ranging from 50 to 200 µg/ml for up to 7 days. We measured cell death by the uptake of Sytox Green (SG), a vital dye that easily penetrates cells with compromised plasma membrane. The quantification of cell death was performed by flow cytometry in SH-SY5Y cells (Fig. 2, Fig. S3). The results showed a time-and-concentration-dependent toxicity of $MAPbI_3$ in this cell line.

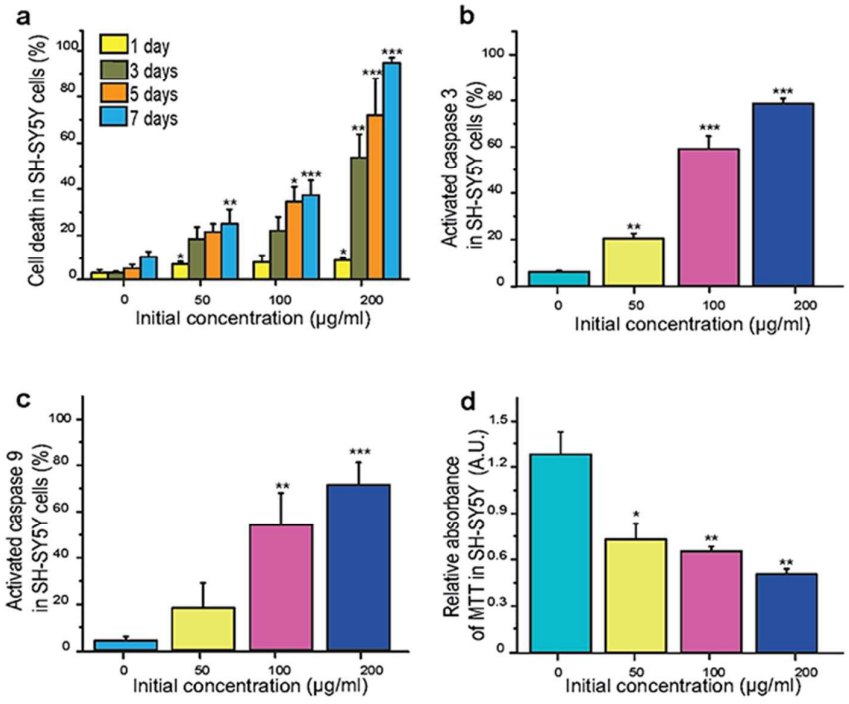

Fig 2. $MAPbI_3$ induces intrinsic apoptosis in SH-SY5Y neuroblastoma cells.
The cells were plated in 24 wells and treated with increasing concentrations of $MAPbI_3$ (50, 100 and 200 µg/ml). **(a)** Cell death was measured by flow cytometry using the fluorescent vital probe Sytox Green (SG), which enters only cells with damaged plasma membrane. Cell death level is expressed as the percentage of cells with compromised cell membrane (SG positive

cells) to the total cell number; **(b-c)** The apoptotic pathways activated by $MAPbI_3$ were identified by measuring the caspase 3 and caspase 9 activities after 5 days of treatment using fluorogenic assays; **(d)** The metabolic activity of the SH-S5Y5 was determined by MTT assay at 5 days post-treatment for increasing concentrations of $MAPbI_3$.
All the histograms show an average of at least 3 independent repeats (each condition in triplicate). Bars are means ± S.D. One-way ANOVA test followed by a Tukey-Kramer post-hoc test were performed (non-treated vs. $MAPbI_3$ treated conditions), *p<0.01, **p<0.005, ***p<0.0005.

Exposure of SH-SY5Y cells to $MAPbI_3$ at a concentration as low as 50 µg/ml, was sufficient to trigger significant cell death (from 10 to 30%) after 7 days, whereas at the highest concentration (200 µg/ml) of $MAPbI_3$, more than half of the SH-SY5Y cell population was dead 3 days post-treatment, and almost all of them did not resist the treatment after 7 days (Fig. 2a, Supplementary Fig. S4a).

To validate our findings we next investigated the effect of $MAPbI_3$ in the differentiated mice hippocampal primary neurons. These neurons have the advantage to spontaneously differentiate in their growth cell culture medium after two week in culture[31] allowing long term toxicity studies (up to four weeks). $MAPbI_3$ was added to the cell culture medium of the primary hippocampal neurons at various concentrations and up to 25 days. Figure 3a showed that $MAPbI_3$ also induced cell death in a time- and concentration-dependent manner in these cells.

Next, we sought to investigate the molecular mechanisms by which $MAPbI_3$ induced death in these two neuronal models. Using fluorogenic assays combined with flow cytometry, we observed that caspase 3, a key enzyme involved in the execution phase of apoptosis, was significantly activated in SH-SY5Y cells exposed for 5 days to $MAPbI_3$ (Fig. 2b). To be noted that necrotic cell death was not induced under these conditions (Supplementary Fig. S5). In order to elucidate the $MAPbI_3$-mediated apoptotic pathways, we monitored the activation of the caspase 8, a key initiator caspase activated by the extrinsic/death receptors pathway, and the caspase 9, a key initiator caspase activated by the intrinsic/mitochondrial pathway. Figure 2c demonstrates a concentration-dependent caspase 9 activation in SH-SY5Y cells treated for 5 days with $MAPbI_3$.

No increase in caspase 8 activity was observed under the same conditions (Supplementary Fig. S4b). This finding suggests that apoptosis in SH-SY5Y cells is triggered through the mitochondrial pathway. To confirm this result, we finally quantified the metabolic activity of the SH-SY5Y cells exposed to $MAPbI_3$ using 3-(4,5-dimethylthiazol-2-yl)-2,5-diphenyltetrazolium bromide MTT assay normalized to the cells confluence. We found a clear decrease in mitochondrial activity in SH-SY5Y cells exposed to $MAPbI_3$ for 5 days (Fig. 2d), confirming mitochondrial dysfunction.

The specific activation of the caspase 3 (Fig. 3b) and the caspase 9 (Fig. 3c) together with the absence of caspase 8 (Fig. 3d) and the decrease in mitochondrial activity (Fig. 3e) also confirmed the initiation of the intrinsic apoptotic pathway in the differentiated hippocampal primary neurons exposed to $MAPbI_3$ as already monitored in SH-SY5Y cells.

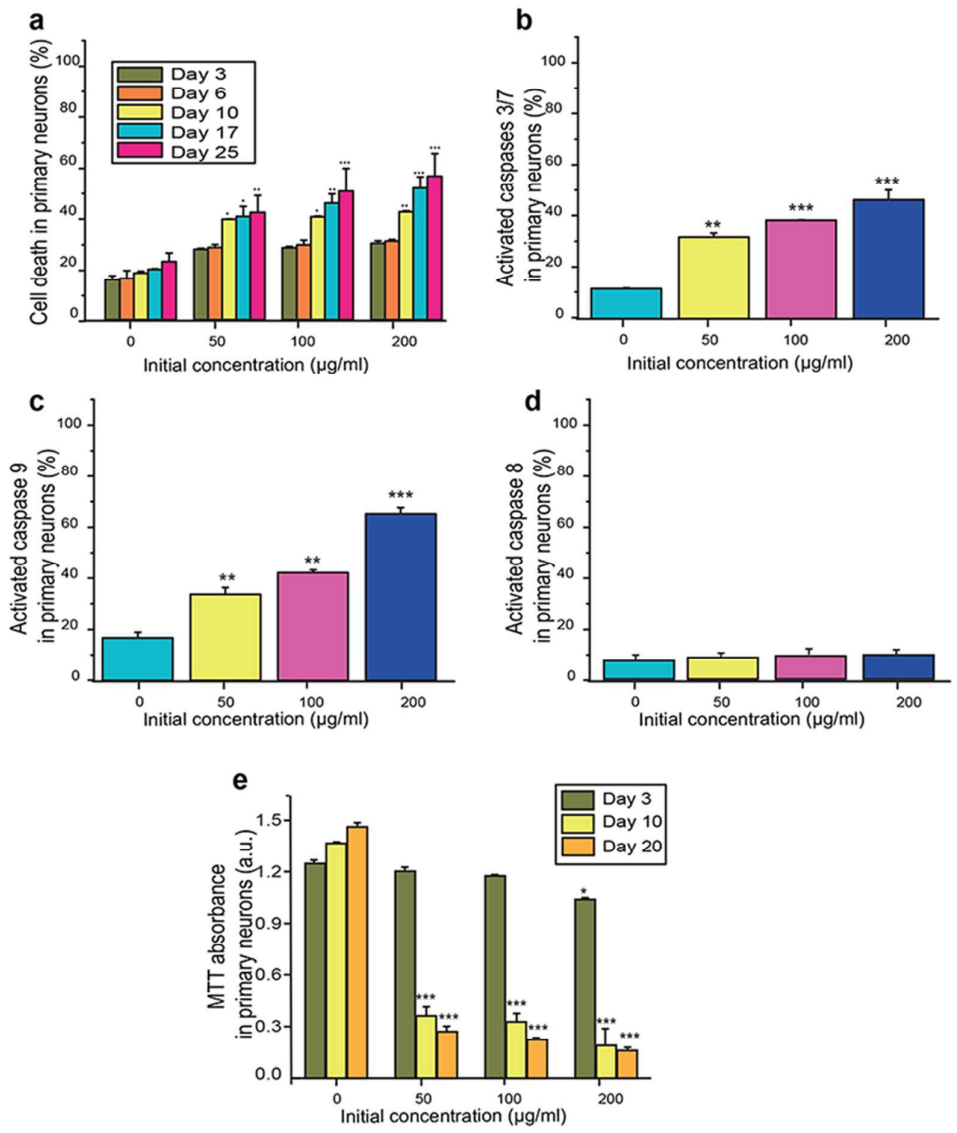

Fig 3. $MAPbI_3$ induces apoptosis in differentiated mice primary hippocampal neurons. Neurons were plated in a 96-well plate. Once differentiated (2 weeks post-plating), primary neurons were treated with increasing concentrations of $MAPbI_3$ [50, 100 and 200 µg/ml] and the cellular toxicity was evaluated using complementary cell death assays. **(a)** Cell death was measured by plate reader (487nm/519nm) using the fluorescent vital probe Sytox Green (SG), which only penetrates cells with damaged plasma membranes. Cell death level is expressed as the percentage of cells with compromised cell membrane (SG positive cells) to the total cell number; **(b-d)** Caspase 3, caspase 9 and caspase 8 activities were measured at 20 days of treatment using fluorogenic assays combined to a plate reader (487nm/519nm) quantification; **(e)** The metabolic activity was determined by MTT assay at 3, 10 and 20 days of treatment. Absorbance at 570 nm was quantified by plate-reader. These observations corroborate with the results obtained on SH-SY5Y neuron cell line.

All the histograms show an average of at least 3 independent repeats (each condition in triplicate). Bars are means ± S.D. One-way ANOVA test followed by a Tukey-Kramer post-hoc test were performed (non-treated vs. $MAPbI_3$ treated conditions), *p<0.05, **p<0.005, p***<0.0005.

2.3 $MAPbI_3$ alters the proliferation capacity and mitochondrial activity of A549 cells without inducing cell death.

Figure 4a shows the absence of Sytox Green uptake by A549 cells upon $MAPbI_3$ exposure, which suggests that the plasma membrane integrity of this cell line is not compromised over the treatment (Fig. 4a and Fig. S6). These findings are consistent with the lack of significant activation of caspases 3, 8 and 9 upon treatment with $MAPbI_3$ (50-200 µg/ml) (Fig. 4b).

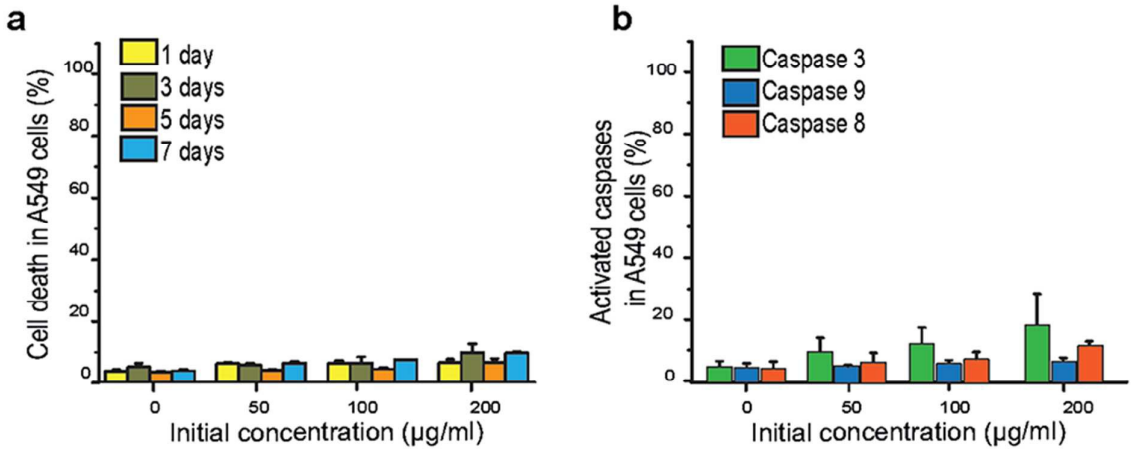

Fig 4. $MAPbI_3$ does not induce cell demise in A549 human lung epithelial cells.

The cells were treated with increasing concentrations of $MAPbI_3$ (50, 100 and 200 µg/ml) and the cellular toxicity was evaluated using flow cytometry **(a)**. A549 cells were harvested after 1, 3, 5 or 7 days post-treatment and stained with SG. Cell death level is expressed as the percentage of cells with compromised cell membrane (SG positive cells) to the total cell number **(b)** A549 cells were harvested 5 days post-treatment and caspase 3, caspase 9 and caspase 8 activities were measured using fluorogenic assays.

All the histograms show an average of at least 3 independent repeats (each condition in triplicate). No significance was observed.

After 5 days of culture, the non-treated A549 cells reached confluency whereas the density of the cells exposed to $MAPbI_3$ decreased significantly (4 times less) in a concentration-dependent manner (Fig. 5a). Interestingly, imaging by bright field optical microscopy (Fig. 5b) and immunocytochemistry (Fig. 5c) revealed a heterogeneous population of cells with different morphologies. The non-treated cells exhibited a homogenous triangle-shape with an average size ranging from 15 to 20 µm, typical of epithelial cells. After 5 days of exposure to $MAPbI_3$, we observed different cell populations in morphology (Fig. 5c): the overall size of some cells significantly increased (“giant cells”, size >50 µm) with a round-shaped aspect. Some cells were stretched and acquired an elongated morphology (“elongated cells”, width < 7 µm).

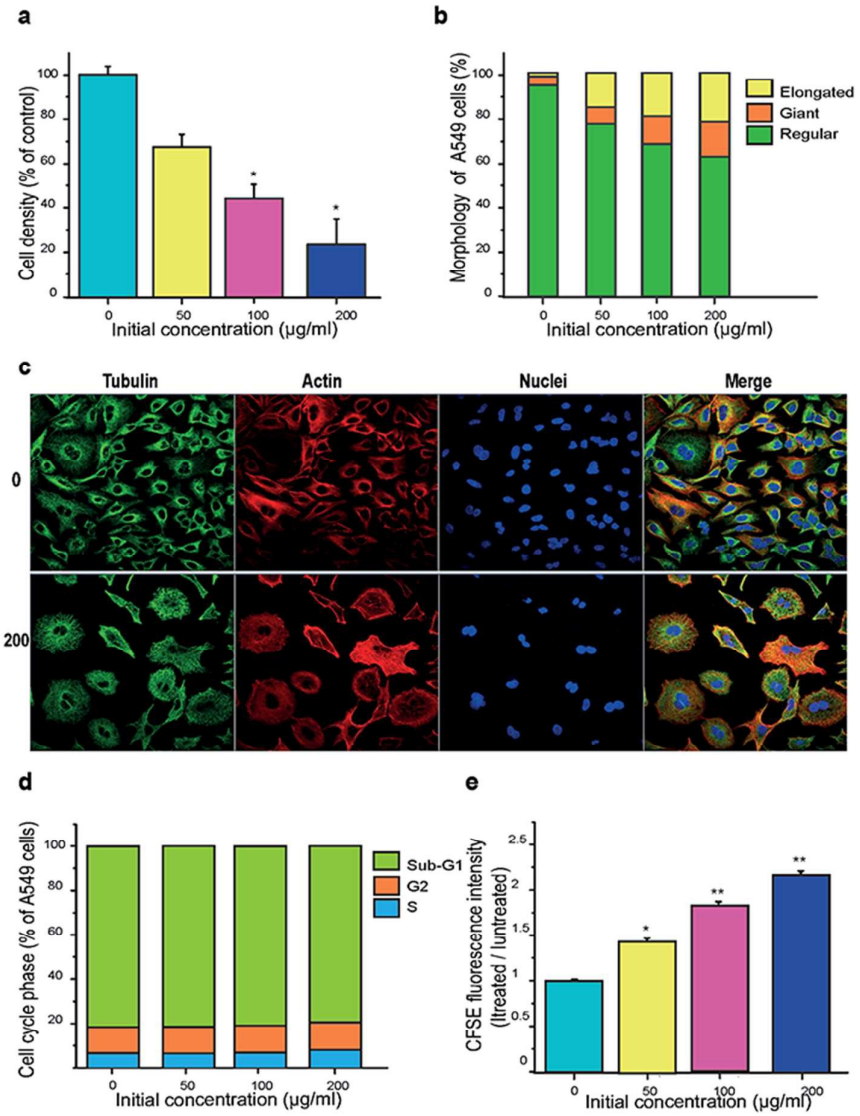

Fig 5. Morphological and proliferation changes caused by $MAPbI_3$ in A549 human lung epithelial cells.

Cells were treated during 5 days with increasing concentrations of $MAPbI_3$ (50, 100 and 200 µg/ml) and the cellular changes were evaluated using complementary assays. **(a)** Variation of the cellular density evaluated using a Neubauer hemocytometer; **(b)** Morphological changes observed by bright field optical microscopy were quantified then normalized to non-treated cells, which have an overall triangle-shaped form and a size between 15 and 20 µm. The size significantly increased ("giant cells", size > 50 µm) in treated cells and became rounded. Some cells acquired a stretched/elongated morphology ("elongated cells", width < 7 µm). An average of 500 cells were counted for each condition tested; **(c)** Tubulin and actin distribution: A549 cells were immunostained against β-tubulin (green), actin (red) and nuclei using DAPI (blue), then imaged using confocal microscopy. Non-treated condition is shown on the top panel and

treated cells on the bottom panel. Scale bars=10 μm; **(d)** Cell cycle (sub-G1, S and G2) distribution assessed by flow cytometry: the histograms show the distribution of sorted cells based on their DNA content which did not change even at the highest concentration of $MAPbI_3$; **(e)** Proliferation capacity assessed using flow cytometry, the fluorescence intensity of CFSE in treated cells is normalized to the non-treated ones.
All the histograms show an average of at least 3 independent repeats (each condition in triplicate). Bars are means ± S.D. One-way ANOVA test followed by a Tukey-Kramer post-hoc test were performed (non-treated vs $MAPbI_3$ treated conditions), *p<0.05 and **<0.001.

One could hypothesize that the decrease in cell density is due to the changes in cell division cycle of the A549 exposed to $MAPbI_3$. However, Fig 5c shows that the organization of actin and tubulin[32] (network of proteins of the cytoskeleton that is rearranged during cell division) was not affected in A549 cells exposed to $MAPbI_3$ suggesting that there is no major difference in the cell division process between the two conditions. This is confirmed by detailed measurements of the sub-G1, S and G2 cell cycle phases (in simple terms, growth phase after the mitosis, DNA replication and maturation before the cell division, respectively) using flow cytometry. The distribution of cell cycle phases was similar between the non-treated and treated cells with various concentrations of $MAPbI_3$ after 5 days (Fig. 5d).

Since the proportion of A549 cells in the different cell cycle phases remained unchanged after $MAPbI_3$ treatment, we sought to determine if the kinetics of the proliferation were altered by measuring the fluorescence intensity of the Carboxy Fluorescein Succinimidyl Ester (CFSE) dye by flow cytometry. This dye diffuses passively into cells and its intensity decreases by half after every cell division cycle. The results in Fig. 5e show the fluorescence intensity of the CFSE normalized to non-treated cells after 5 days of exposure for increasing concentrations of $MAPbI_3$. Cells exposed to the highest concentration of $MAPbI_3$ showed a CFSE fluorescence intensity that is 2.3 times higher than non-treated cells, suggesting that division kinetics have decreased in $MAPbI_3$ treated cells which is the reason for their slower proliferation.

To gain more detailed insight into the molecular and cellular basis of $MAPbI_3$-induced cellular dysfunction, we examined the effect of $MAPbI_3$ on the cellular compartments and architecture of the A549 cells using TEM.

As shown in Figure 6 (a, b), treatment with $MAPbI_3$ resulted in increased size of cells, multiple nuclei, increased number of lamellar bodies and mitochondrial damage. The multiple nuclei present in the treated cells did not show any ultra-structural defects with well-preserved nuclear membrane and also present multiple nucleoli. Interestingly, in treated cells, the density of lamellar bodies (LB), secretory organelles that store lung surfactants[33], markedly amplified.

However, the most striking effect of $MAPbI_3$ treatment was observed on the mitochondrial compartment. The non-treated cells showed typical ultrastructure of the mitochondrial cristae organization (Fig. 6c, light green), whereas cells treated with $MAPbI_3$ exhibited severely damaged mitochondria (Fig. 6d). The size of mitochondria in these cells increased dramatically and the intra-mitochondrial space became highly dilated with severe damage to the cristae organization (Fig. 6d, dark green). These results suggest that $MAPbI_3$ induces adverse effects on the mitochondrial function of A549 cells.

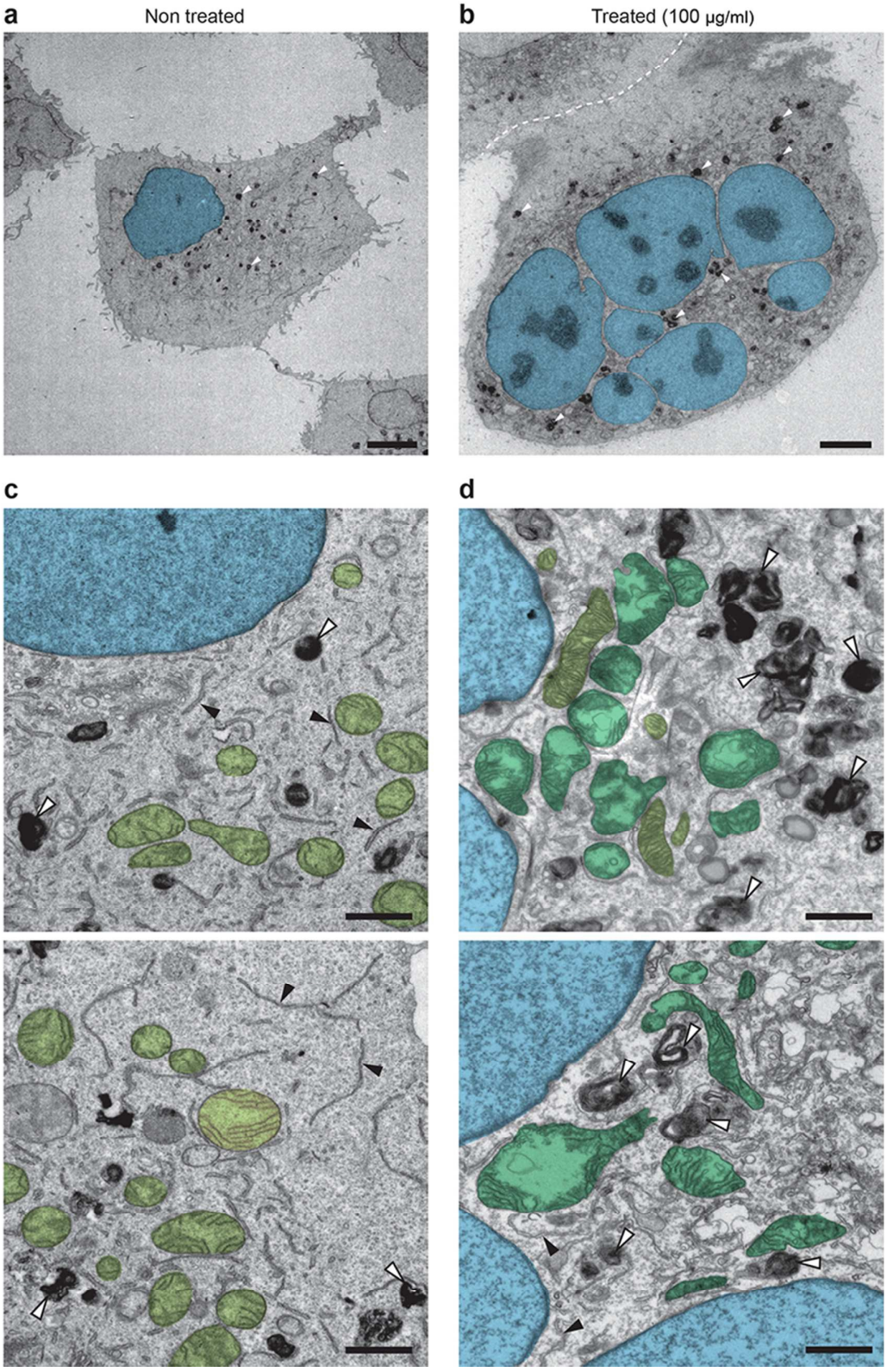

Fig 6. Ultrastructural analysis of A549 cells.

(a) Low magnification electron micrograph of the non-treated A549 cells grown in monolayer on the plastic Thermanox coverslip and processed for the electron microscopy. A typical cellular morphology is shown with single nucleus (blue) well preserved nuclear membrane and multiple nucleoli and lamellar bodies (LB; white arrows); **(b)** Changed morphology of the A549 cells upon the treatment with $MAPbI_3$ nanoparticles. Low magnification overview image of the large "giant" multinucleated cell containing 7 nuclei and significantly increased number of lamellar bodies depicted by white arrows; **(c)** Two characteristic higher magnification images of the normal mitochondrial (green) morphology with typical cristae organization, tubular organization of the endoplasmic reticulum (black arrowheads) together with lamellar bodies (white arrows); **(d)** Two characteristic higher magnification images demonstrating the severe damage of the mitochondria, particularly increased their size compared to the non-treated A549 cells and highly dilated intra-mitochondrial space and reduced cristae organization. The lamellar bodies (white arrows) and tubular organization of the endoplasmic reticulum are marked (black arrowheads). Scale bars: 5 μm in **a** and **b**; 1 μm in **c** and **d.**

To test this hypothesis, we assessed the effect of $MAPbI_3$ on mitochondrial function using different assays. We observed a time and $MAPbI_3$ dose-dependent increase of the mitochondrial activity using the MTT assay (Fig. 7a). We then compared the mitochondrial membrane potential ($\Delta\Psi_m$) in the non-treated and treated cells by measuring the capacity of Mitotracker Red CMXRos to be taken up and retained into the mitochondria. Figure 7b shows a significant increase of the $\Delta\Psi_m$ in the cells exposed to $MAPbI_3$. Finally, we measured the overall mass of the mitochondria, assessed using the Mitotracker green FM and flow cytometry, which was also slightly increased in the treated cells (Fig. 7c).

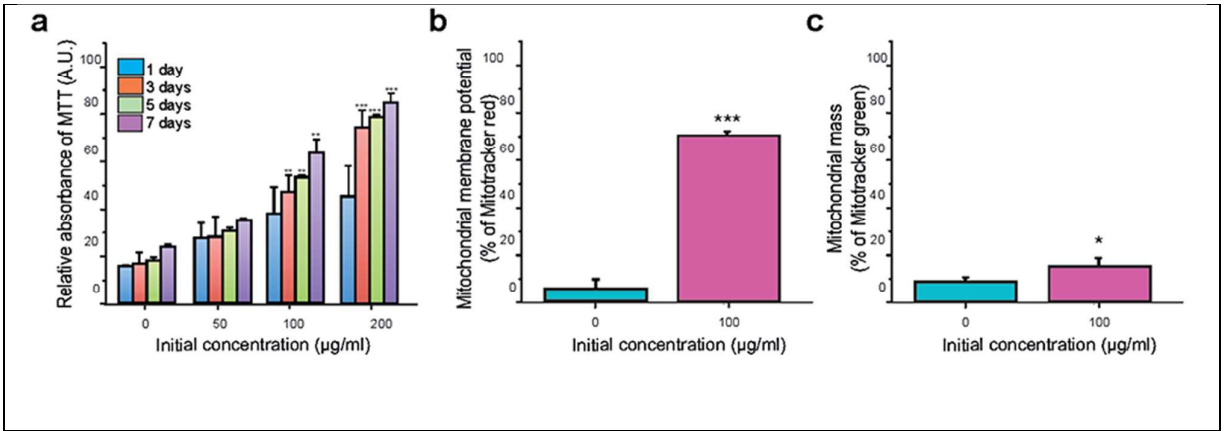

Fig 7. Effect of $MAPbI_3$ on the mitochondrial function of A549 cells.
A549 cells were treated with increasing concentrations of $MAPbI_3$ (50, 100 and 200 µg/ml) and their mitochondrial activity was evaluated. **(a)** MTT assay after 1, 3, 5 and 7 days of exposure to $MAPbI_3$ showing increasing metabolic activity normalized to number of counted cells; (**b)** Mitochondrial membrane potential ($\Delta\Psi_m$) was assessed in non-treated and treated cells (100 µg/ml of $MAPbI_3$) at 5 days post-treatment. Cells were stained by Mitotracker Red CMXRos and analyzed by flow cytometry. These results corroborate with the increased mitochondrial activity seen in **a; (c)** Overall mass of mitochondria was measured in non-treated and treated cells (100 µg/ml of $MAPbI_3$) at 5 days post-treatment. Cells were stained by Mitotracker Green and analyzed by flow cytometry.
All the histograms show an average of at least 3 independent repeats (each condition in triplicate). Bars are means ± S.D. One-way ANOVA test followed by a Tukey-Kramer post-hoc test were performed (non-treated vs $MAPbI_3$ treated conditions), *p<0.05, **p<0.005 and ***<0.0005.

In summary, $MAPbI_3$ does not induce the cell death of human lung epithelial cells but heavily affects their phenotype, proliferation kinetics and the mitochondrial activity, potential and mass. The effects of $MAPbI_3$ on human lung epithelial cells were markedly different compared to the neuronal cells.

3. Discussion

The discovery of perovskite as a cheap and extremely efficient material to convert sunlight to electricity represents a major breakthrough in the development of photovoltaic cells. Manufacturing companies are already planning to commercialize this novel material in the near future. However, one serious drawback of the large scale exploitation of the perovskite is its lead content that raises major concerns[1] about its potential toxicity during device production, handling and disposal.

In our study we observed that when $MAPbI_3$ is dispersed in cell culture media a part forms a precipitate, while 6% of its lead and more than 90% of its iodine contents stay in solution (see Fig. 1). Methylamine is known to be highly soluble in a water-rich environment.[30] In this study, we considered the soluble part of $MAPbI_3$ only. Herein, we showed that $MAPbI_3$ perovskite caused a

time-and-dose-dependent toxicity in both SH-SY5Y neuroblastoma cell line and in differentiated mice primary hippocampal neurons. In both neuronal cell types, $MAPbI_3$ damaged the plasma membrane and triggered apoptotic cell death via the activation of the mitochondrial/intrinsic pathway signaled by caspase 9. Lead could be the main cause of this effect since it is known to depolarize cells mitochondria resulting in cytochrome c release, caspases activation, and apoptosis.[31,32] In humans, a blood lead level >0.1 µg/ml is considered to be elevated even though clinical symptoms are rarely seen below 0.6 µg/ml in chronic poisoning[12]. Moreover, *in vivo*, the accumulation of lead in the organism amplifies the toxic effect. In our *in vitro* cellular studies the effect of accumulation was substituted by the increased concentration. It is known that lead is a neurotoxin which is considered to be a major global environmental health hazard. Molecular epidemiology studies showed that chronic exposure to lead was associated with an increased risk of amyotrophic lateral sclerosis[34], Parkinson disease[35] and late-onset Alzheimer's disease[36]. Although there are many investigations, the mechanisms underlying lead toxicity are still a matter of active research. However, not only lead is released when the $MAPbI_3$ is dissolved in organic fluid, but also Iodide and Methylamine. Interestingly, methylamine is also known to be toxic since it exerts adverse effects on fetal development and embryo survival in mice.[25]

Remarkably, in the case of epithelial cells such as A549 human lung cells, exposure to $MAPbI_3$ did not result in cell death, but the proliferation rate decreased without cell cycle arrest leading to severe morphological changes and significant increase in the mitochondrial mass and activity. Upon exposure to $MAPbI_3$, A549 cells became giant and polynucleated; their mitochondria showed an unusual polymorphic arrangement of the cristae. Lead ions are known to enter some cells through calcium channels, then bind to calmodulin (with a higher affinity than calcium) which alters enzyme activities, gene transcription and cell signaling.[16,28] On the other hand, methylamines are also known to inhibit protein turnover resulting in a modification the cells' DNA and RNA content.[25]

The solubility of $MAPbI_3$ could be at the origin of the polynuclearity and the modified mitochondria. Paradoxically, the metabolic activity rate produced by the mitochondria increased significantly in response to $MAPbI_3$ exposure (Fig. 7), whereas cell proliferation kinetics and

confluency decreased. At first sight, this observation seems controversial but as the cells become giants and escape death, they must expand their energy production for survival. Mitochondria are essential regulators of metabolism, stress responses, cell survival and cell death.[37,38]

One reason for the different response of the epithelial and neurons to $MAPbI_3$ exposure might be the presence of lamellar bodies in the former ones and their absence in the latter cells. These structures are naturally present in the cytoplasm of mucosal cells; they are part of the cellular protective mechanisms against environmental influences[33] of the lung alveoli. A549 cells exposed to $MAPbI_3$ show an increase in the number of lamellar bodies in the cytoplasm. A similar increased number of lamellar bodies was observed in epithelial cells exposed to single-walled carbon nanotube exposure[39]. The cell survival strategies involve countless coordinated physiological and genetic changes that serve to escape cell demise[37]. It seems that one of these strategies consists of increasing the number of lamellar bodies which have a protective function. Genome profiling of treated and non-treated cells may provide a better understanding of the cellular mechanisms underlying the differences in cellular toxicity and cellular phenotypes observed in SH-SY5Y cells, differentiated hippocampal primary neurons and A549 cells.

Finally, our findings are alarming and stress the potential health impact of large-scale production and application of hybrid halide perovskites. Here we inherently assumed that the toxic effect of $MAPbI_3$ comes from the Pb^{2+} ions. But it is also known that methylamine can be toxic[23,25], as well. This suggests that in the search for compositions where lead is replaced by lighter and presumably less toxic elements (e.g. tin), one should also consider alternatives for the cation other than methylamine.

Acknowledgement

Authors address their acknowledgements to SNSF, FCCF core facility at EPFL, Sylvain Coudret, EPFL (ICP-OES), Prof. Gönczy (for providing tubulin antibody), Nathalie Jordan (primary culture) and Prof. Beat Schwaller (for providing A549 cell line). The work of I.B. is supported by the Swiss National Science Foundation for Scientific Research (Grant # 200020_156981).

Experimental methods

Antibodies and compounds

The mouse anti-β-tubulin was purchased from Sigma Aldrich (Switzerland). The Alexa Fluor 594 labelled phalloidin (phalloidin^{AF594}), the secondary antibody donkey anti-rabbit Alexa^{488}, the propidium iodide (PI) dye, the CarboxyFluorescein Succinimidyl Ester (CFSE) proliferation dye, the sytox green dead cells dye, the Mitotracker green dye, the MitoTracker CMXRos Red dye, the polyvinyl alcohol mounting medium with DABCO (PVA), the phosphate buffer saline solution (PBS) and all the cell culture media reagents were purchased from Life Technology (Switzerland). The CaspaTag^{TM} fluorescein caspase 3, 8 or 9 activities kit were purchased from Enzo Life Sciences (Switzerland). Tetrazolium derivative 3-[4,5- dimethylthiazol-2-yl]-2,5-diphenyl tetrazolium bromide (MTT) was purchased from Sigma-Aldrich (Switzerland).

Scanning Electron Microscopy (SEM) imaging

Scanning Electron Microscope images were acquired with a MERLIN Zeiss electron microscope. The elemental composition of the $MAPbI_3$ crystallites and its solid decomposition byproducts were analyzed by EDS. Energy-dispersive X-ray spectroscopy (EDS) measurements were done with an X-MAX EDS detector mounted at a 35 degree take-off angle with a SATW window. EDS spectra were taken at a working distance of 8.5 mm with 20 keV accelerating voltage and a current held at 200 pA.

Inductively Coupled Plasma Atomic Emission Spectroscopy (ICP-AES)

The solubility of $MAPbI_3$ polycrystalline powder was determined in deionized water as well as in two types (DMEM and DMEM:F12) of cell culture medium by using Inductively Coupled Plasma Atomic Emission Spectroscopy (ICP-AES). 3.04 mg of $MAPbI_3$ crystals were dispersed in 10 ml of deionized water and cell culture medium (DMEM and DMEM:F12), respectively. Aliquots were taken at various time points (1-5 days), and filtered using 0.22 um pore cellulose filters (Merck Millipore, Switzerland). The lead and iodine concentrations of the clear and transparent solutions were analyzed using Inductively Coupled Plasma Optical Emission Spectroscopy (Shimadzu ICPE-9000). Each sample was analyzed in triplicate.

Culture of mammalian cell lines

A549 Type II human alveolar basal epithelial cells were cultured in DMEM medium (Life Technologies) supplemented with 10% fetal bovine serum (FBS) and 1% Penicillin/Streptomycin (P/S). The human neuroblastoma SH-SY5Y cell line was cultured in a DMEM: F12 (Life Technologies) supplemented with 10% FBS and 1% P/S. Both cell lines were cultured in a humidified 5% CO_2 atmosphere at 37°C and respectively plated at a density of 13,000 and 24,000 cells per well in 24 wells transparent plate (BD biosciences, Switzerland) for further analysis.

Culture of mice primary hippocampal neurons

Hippocampal neurons were prepared from P1 mice pups (Harlan Laboratories) as previously described by Steiner et al.[40] and were plated at a density of 30'000 cells per well in 96 wells plates, coated with poly-L-Lysine, in growth medium (minimum Eagle's medium with 20 mM glucose, 0.5 mM glutamine, 100 units/mL penicillin, 100 µg/mL streptomycin, 10% horse serum). The neurons were used once differentiated (two weeks after plating): in growth media, the hippocampal primary neurons will develop overtime axonal and dendritic arbores that can be positively stained respectively with MAP2 and Tau markers. Hippocampal primary neurons are considered as post-differentiated after 2 weeks in culture.[31]

Preparation of conditioned medium for treatment

5 days before administration to cells, $MAPbI_3$ was suspended at concentrations of 50, 100 and 200 µg/ml in preheated culture medium. Solutions are prepared at RT and vortexed under laminar flow. They remain 5 days at RT, then filtered at 220 nm pore size filter (Merck Millipore, Switzerland) then stored at 4°C.

Quantification of cell death by dye exclusion method in mammalian cell lines

SH-SY5Y cells and A549 cells were plated in 24 wells plates. The following day, the original culture medium was removed from the cells and replaced by medium spiked with increasing concentrations of $MAPbI_3$ (50, 100 and 200 µg/ml). After 1, 3, 5 or 7 days of exposure, cell death was quantified using the vital dye Sytox Green (SG) which only penetrates in cells with damaged plasma membrane. The supernatant and adherent cells were collected at each indicated time point. After 5 min of centrifugation at 250 g, cells were re-suspended in PBS containing SG at a final concentration of 330 nM. Cells were then analyzed (20'000 events per condition were counted) by flow cytometry using Accuri C6 (BD Biosciences, Switzerland). SG emission was collected in FI1 channel and FlowJo software (Treestar, USA) was used for subsequent analysis.

Quantification of cell death by dye exclusion method in primary hippocampal neurons exposed to $MAPbI_3$

Hippocampal primary neurons were plated in 96 wells plate. After 2 weeks of culture, the original culture medium was removed from the cells and replaced by medium spiked with increasing concentration of $MAPbI_3$ (of 50, 100 and 200 µg/ml). Cell death was quantified as previously described by Mahul-Mellier et al.[41] using the vital dye exclusion method using Sytox Green (SG, Life Technology, Switzerland), a membrane impermeable dye which will enter only in cells with damaged plasma membranes after 3, 10, 17 and 25 days of exposure to $MAPbI_3$. Briefly neuronal cells were washed 3 times with PBS before being incubated with SG at a final concentration of 330 nM. After 15 minutes of incubation, cells were washed twice with PBS and fluorescence was

quantified using by using Tecan infinite M200 Pro plate reader (Tecan, Switzerland) with respective excitation and emission wavelength of 487 nm and 519 nm.

Quantification of active caspase 3, 8 and 9 in mammalian cell lines and in hippocampal primary neurons

SH-SY5Y cells and A549 cells were plated in 24 wells plates. The following day, the original culture medium was removed from the cells and replaced by medium spiked with increasing concentrations of $MAPbI_3$ (50, 100 and 200 µg/ml). Caspases activity in living cells was quantified using CaspaTag^{TM} fluorescein caspase 3, 8 or 9 activities kit (Enzo life sciences, Switzerland). These fluorogenic kits used specific Fluorochromes peptide Inhibitors of Caspases (FLICA). These probes passively enter the cells and bind irreversibly to the active caspases. After 5 days of exposure to $MAPbI_3$, SH-SY5Y and A549 cells were harvested and incubated for one hour at 37°C with FAM-DEVD-FMK (caspase 3), FAM-LETD-FMK (caspase 8) or FAM-LEHD-FMK (caspase 9) and with the vital dye Propidium Iodide (PI) in accordance with the supplier's instructions. Fluorescein emission was analyzed by flow cytometry [Accuri C6 (BD Biosciences)] in Fl1 channel and PI emission was collected in Fl3 channel. FlowJo was used for subsequent analysis.

For hippocampal primary neurons, cells were plated in 96 wells plate. After 2 weeks of culture, the original culture medium was removed from the cells and replaced by medium spiked with increasing concentrations of $MAPbI_3$ (50, 100 and 200 µg/ml). Neurons were washed 3 times with PBS and incubated for 30 minutes at 37°C with FAM-DEVD-FMK (caspase 3), FAM-LETD-fmk (caspase 8) or FAM-LEHD-fmk (caspase 9) in accordance with the supplier's instructions. Fluorescein emission was quantified by using Tecan infinite M200 Pro plate reader (Tecan, Switzerland) with respective excitation and emission wavelength of 487 nm and 519 nm.

Quantification of the metabolic activity of mammalian cell lines and hippocampal primary neurons

SH-SY5Y and A549 cells were plated in 24-well plates and hippocampal primary neurons in 96 well plates. The following day, the original culture medium was removed from the cells and replaced by medium spiked with increasing concentrations of $MAPbI_3$ (50, 100 and 200 µg/ml). Metabolic activity of the cells was measured using the tetrazolium derivative 3-[4,5-dimethylthiazol-2-yl]-2,5-diphenyl tetrazolium bromide (MTT) assay. This colorimetric assay based on the capacity of the healthy cells to reduce MTT (Sigma Aldrich, Switzerland) in a purple formazan product. Briefly, after the indicated days of exposure to $MAPbI_3$, 5 mg/ml MTT was added to the different cell cultures. After 3 hours of incubation, the culture medium was aspired and replaced by 100 µl or 20 µl (respectively in 24 or 96 wells plate) of DMSO (Sigma-Aldrich). The levels of formation of formazan products were quantified by using Tecan infinite M200 Pro plate reader (Tecan). Absorbance of the converted dye was measured at a wavelength of 570 nm with background subtraction at 630–690 nm. Normalization to the number of counted cells had to be performed, in order to take into account both the changes in proliferation and the confluence of A549 and SH cells and thus to fit the measured MTT absorption to the relative mitochondrial activity.

Counting of the A549 and SH-SY5Y cells density

Cells were plated in 24-well plates. The following day, the original culture medium was removed from the cells and replaced by medium spiked with increasing concentrations of $MAPbI_3$ (50, 100 and 200 µg/ml). After 5 days of exposure, cell titer was quantified using a Neubauer hemocytometer chamber. Cells were harvested after trypsin treatment (Life Technologies) and 10 µl of the cell suspension was placed in the counting chamber.

Quantification of the morphological alterations of A549 cells

A549 cells were plated in 24-well plates. The following day, the original culture medium was removed from the cells and replaced by medium spiked with increasing concentrations of $MAPbI_3$

(50, 100 and 200 µg/ml). A549 cells were imaged 5 days after exposure to various concentrations of $MAPbI_3$ on an EVOS bright field microscope (Life Technologies). The respective sizes and shapes of the cells were analyzed using FIJI software (NIH, Bethesda, MD, USA).

Quantification of the cell cycle distribution of A549 cells

A549 cells were plated in 24-well plates. The following day, the original culture medium was removed from the cells and replaced with a medium spiked with increasing concentration of $MAPbI_3$ (50, 100 and 200 µg/ml). After 5 days of exposure, the cell cycle was analyzed using propidium iodide (PI) staining (Life Technologies). Cells were harvested using the classical trypsin (Life Technologies) procedure. After 5 minutes of centrifugation at 200 *g* at 4°C, cells were suspended in ice-cold buffer, gently mixed then added to an equal volume of cold absolute ethanol and stored at 4°C for 24 hours. Cells were then centrifuged for 10 minutes at 200 *g* and washed with cold PBS. The pellets were resuspended in cold PBS containing 0.1 % (v/v) Triton X-100 (Sigma-Aldrich) and 0.4 % (v/v) 5 µg/ml PI (which allows the cellular DNA content staining). Cell cycle distribution was analyzed (15'000 events per condition were measured) by flow cytometry using Accuri C6 (BD Biosciences). PI emission was collected in Fl2 channel and FlowJo software (Treestar) was used for subsequent analysis.

Quantification of cell proliferation of A549 cells

A549 cells were plated in 24-well plates and the medium was replaced by PBS containing CFSE proliferation dye (Life Technologies) at a final concentration of 5 µM and left for 10 minutes at 37^0C then rinsed with PBS and left in complete medium overnight. The following day, medium was removed from the cells and replaced with a medium spiked with increasing concentrations of $MAPbI_3$ (50, 100 and 200 µg/ml). After 0, 1, 3 and 5 days of exposure, treated and non-treated A549 cells were harvested using trypsin procedure and PI was added to the cells suspension. Cell proliferation capacity was then analyzed (15'000 events per condition were measured) by flow cytometry using Accuri C6 (BD Biosciences). CFSE emission was collected in Fl1 channel and FlowJo software (Treestar) was used for subsequent analysis.

Immunocytochemistry (ICC)

A549 cells were seeded onto coverslips coated with poly-L-lysine (Life Technologies) and treated with $MAPbI_3$ at a final concentration of 200 µg/ml. After the treatment, cells were washed 3 times with PBS and then fixed in 4% PFA (paraformaldehyde, Sigma-Aldrich) for 20 min at RT. After blocking with 3% BSA (Bovine Serum Albumin) in 0.1% Triton X-100 PBS (Phosphate Buffer Saline) (PBST) for 30 minutes at RT, cells were incubated with the rabbit anti-β-tubulin primary antibody for two hours at RT. The cells were rinsed five times in PBST and subsequently incubated with the secondary anti-mouse $Alexa^{488}$ at a dilution of 1/800 in PBST and with the labelled $phalloidin^{AF594}$ at a dilution of 1/1000 in PBST. The cells were washed five times in PBST and incubated 30 minutes at RT in DAPI at 2 µg/ml, before mounting in polyvinyl alcohol mounting medium with DABCO. The cells were then examined with confocal laser-scanning microscope (LSM 700, Zeiss) with a 40x objective and analyzed using Zen software (Zeiss).

Measurement of the mitochondrial membrane potential changes ($\Delta\Psi_m$) and the overall mass of mitochondria in A549 cells

A549 cells were plated in 24 wells plates. The following day, the original culture medium was removed from the cells and replaced by medium spiked with 100 µg/ml of $MAPbI_3$. After 5 days of exposure, the $\Delta\Psi_m$ was analyzed using the fluorochrome MitoTracker Red (CMXRos) dye, and the overall mass of mitochondria was quantified using the fluorochrome MitoTracker Green. In short, CMXRos is a dye which passively enters in living cells and that is selectively taken up and retained in mitochondria depending on $\Delta\Psi_m$, whereas MitoTracker Green can passively diffusive through the plasma membrane and once inside the cells, this dye selectively binds to the lipids of the mitochondria and fluoresces regardless the mitochondrial membrane potential. Therefore MitoTracker Green allows the overall measurement of the mitochondrial mass.

After 5 days of exposure to $MAPbI_3$, cells were resuspended and incubated for 20 minutes at 37°C with CMXRos and MitoTracker Green in accordance with the supplier's instructions. Mitotrackers emission was analyzed by flow cytometry [Accuri C6 (BD Biosciences)] in Fl2

channel for the CMXRos and in Fl1 channel for the MitoTracker Green, 30’000 events per condition wer5e measured. FlowJo (Treestar) was used for subsequent analysis.

Statistical Analysis

The experiments were independently repeated at least three times in triplicates, yielding the same pattern of results. Statistical analysis was performed using one-way ANOVA followed by a Tukey-Kramer post-hoc test. The data were regarded as statistically significant at $p<0.05$.

References

1. Green, M. A., Ho-Baillie, A. & Snaith, H. J. The emergence of perovskite solar cells. *Nat. Photonics* **8,** 506–514 (2014).
2. Grätzel, M. The light and shade of perovskite solar cells. *Nat. Mater.* **13,** 838–842 (2014).
3. Gao, P., Grätzel, M. & Nazeeruddin, M. K. Organohalide lead perovskites for photovoltaic applications. *Energy Environ. Sci.* **7,** 2448–2463 (2014).
4. Niu, G., Guo, X. & Wang, L. Review of recent progress in chemical stability of perovskite solar cells. *J. Mater. Chem. A* **3,** 8970–8980 (2015).
5. Liu, M., Johnston, M. B. & Snaith, H. J. Efficient planar heterojunction perovskite solar cells by vapour deposition. *Nature* **501,** 395–398 (2013).
6. Malinkiewicz, O. *et al.* Perovskite solar cells employing organic charge-transport layers. *Nat. Photonics* **8,** 128–132 (2014).
7. Nie, W. *et al.* High-efficiency solution-processed perovskite solar cells with millimeter-scale grains. *Science* **347,** 522–525 (2015).
8. Luo, J. *et al.* Water photolysis at 12.3% efficiency via perovskite photovoltaics and Earth-abundant catalysts. *Science* **345,** 1593–1596 (2014).
9. Tan, Z.-K. *et al.* Bright light-emitting diodes based on organometal halide perovskite. *Nat. Nanotechnol.* **9,** 687–692 (2014).
10. Xing, G. *et al.* Low-temperature solution-processed wavelength-tunable perovskites for lasing. *Nat. Mater.* **13,** 476–480 (2014).
11. Hu, X. *et al.* High-Performance Flexible Broadband Photodetector Based on Organolead Halide Perovskite. *Adv. Funct. Mater.* **24,** 7373–7380 (2014).
12. Needleman, H. Lead Poisoning. *Annu. Rev. Med.* **55,** 209–222 (2004).

13. Finkelstein, Y., Markowitz, M. E. & Rosen, J. F. Low-level lead-induced neurotoxicity in children: an update on central nervous system effects. *Brain Res. Brain Res. Rev.* **27,** 168–176 (1998).

14. Toscano, C. D. & Guilarte, T. R. Lead neurotoxicity: From exposure to molecular effects. *Brain Res. Rev.* **49,** 529–554 (2005).

15. Jaishankar, M., Tseten, T., Anbalagan, N., Mathew, B. B. & Beeregowda, K. N. Toxicity, mechanism and health effects of some heavy metals. *Interdiscip. Toxicol.* **7,** 60–72 (2014).

16. Kursula, P. & Majava, V. A structural insight into lead neurotoxicity and calmodulin activation by heavy metals. *Acta Crystallograph. Sect. F Struct. Biol. Cryst. Commun.* **63,** 653–656 (2007).

17. Ibrahim, N. M., Eweis, E. A., El-Beltagi, H. S. & Abdel-Mobdy, Y. E. Effect of lead acetate toxicity on experimental male albino rat. *Asian Pac. J. Trop. Biomed.* **2,** 41–46 (2012).

18. Fowler, B. A., Kimmel, C. A., Woods, J. S., McConnell, E. E. & Grant, L. D. Chronic low-level lead toxicity in the rat: III. An integrated assessment of long-term toxicity with special reference to the kidney. *Toxicol. Appl. Pharmacol.* **56,** 59–77 (1980).

19. Pourrut, B., Shahid, M., Dumat, C., Winterton, P. & Pinelli, E. Lead uptake, toxicity, and detoxification in plants. *Rev. Environ. Contam. Toxicol.* **213,** 113–136 (2011).

20. Hailegnaw, B., Kirmayer, S., Edri, E., Hodes, G. & Cahen, D. Rain on Methylammonium Lead Iodide Based Perovskites: Possible Environmental Effects of Perovskite Solar Cells. *J. Phys. Chem. Lett.* **6,** 1543–1547 (2015).

21. Stoddard II, F. R., Brooks, A. D., Eskin, B. A. & Johannes, G. J. Iodine Alters Gene Expression in the MCF7 Breast Cancer Cell Line: Evidence for an Anti-Estrogen Effect of Iodine. *Int. J. Med. Sci.* **5,** 189–196 (2008).

22. Sherer, T. T., Thrall, K. D. & Bull, R. J. Comparison of toxicity induced by iodine and iodide in male and female rats. *J. Toxicol. Environ. Health* **32,** 89–101 (1991).

23. Mitchell, S. C. & Zhang, A. Q. Methylamine in human urine. *Clin. Chim. Acta Int. J. Clin. Chem.* **312,** 107–114 (2001).

24. Mayer, M. *et al.* Different transport mechanisms in plant and human AMT/Rh-type ammonium transporters. *J. Gen. Physiol.* **127,** 133–144 (2006).

25. Guest, I. & Varma, D. R. Developmental toxicity of methylamines in mice. *J. Toxicol. Environ. Health* **32,** 319–330 (1991).

26. Card, J. W., Zeldin, D. C., Bonner, J. C. & Nestmann, E. R. Pulmonary applications and toxicity of engineered nanoparticles. *Am. J. Physiol. - Lung Cell. Mol. Physiol.* **295,** L400–L411 (2008).

27. Krigman, M. R. Neuropathology of heavy metal intoxication. *Environ. Health Perspect.* **26,** 117–120 (1978).

28. Gillis, B. S., Arbieva, Z. & Gavin, I. M. Analysis of lead toxicity in human cells. *BMC Genomics* **13,** 344 (2012).

29. Poglitsch, A. & Weber, D. Dynamic disorder in methylammonium trihalogenoplumbates (II) observed by millimeter-wave spectroscopy. *J. Chem. Phys.* **87,** 6373–6378 (1987).

30. Roose, P., Turcotte, M. G. & Mitchell, J. W. in *Kirk-Othmer Encyclopedia of Chemical Technology* (John Wiley & Sons, Inc., 2000).

31. Iii, G. M. J. B. *et al.* Culturing pyramidal neurons from the early postnatal mouse hippocampus and cortex. *Nat. Protoc.* **7,** 1741–1754 (2012).

32. Mattila, P. K. & Lappalainen, P. Filopodia: molecular architecture and cellular functions. *Nat. Rev. Mol. Cell Biol.* **9,** 446–454 (2008).

33. Schmitz, G. & Müller, G. Structure and function of lamellar bodies, lipid-protein complexes involved in storage and secretion of cellular lipids. *J. Lipid Res.* **32,** 1539–1570 (1991).

34. Kamel, F. *et al.* Lead exposure as a risk factor for amyotrophic lateral sclerosis. *Neurodegener. Dis.* **2,** 195–201 (2005).

35. Weisskopf, M. G. *et al.* Association of cumulative lead exposure with Parkinson's disease. *Environ. Health Perspect.* **118,** 1609–1613 (2010).

36. Bakulski, K. M., Rozek, L. S., Dolinoy, D. C., Paulson, H. L. & Hu, H. Alzheimer's Disease and Environmental Exposure to Lead: The Epidemiologic Evidence and Potential Role of Epigenetics. *Curr. Alzheimer Res.* **9,** 563–573 (2012).

37. Portt, L., Norman, G., Clapp, C., Greenwood, M. & Greenwood, M. T. Anti-apoptosis and cell survival: A review. *Biochim. Biophys. Acta BBA - Mol. Cell Res.* **1813,** 238–259 (2011).

38. Galluzzi, L., Kepp, O., Trojel-Hansen, C. & Kroemer, G. Mitochondrial Control of Cellular Life, Stress, and Death. *Circ. Res.* **111,** 1198–1207 (2012).

39. Maria Davoren, E. H. In vitro toxicity evaluation of single walled carbon nanotubes on human A549 lung cells. *Toxicol. Vitro Int. J. Publ. Assoc. BIBRA* **21,** 438–48 (2007).

40. Steiner, P. *et al.* Modulation of receptor cycling by neuron-enriched endosomal protein of 21 kD. *J. Cell Biol.* **157,** 1197–1209 (2002).

41. Mahul-Mellier, A.-L. *et al.* Fibril growth and seeding capacity play key roles in α-synuclein-mediated apoptotic cell death. *Cell Death Differ.* (2015).